5-1-2015

Superconductivity versus structural phase transition in the closely related Bi2Rh3.5S2 and Bi2Rh3S2

Udhara S. Kaluarachchi
Iowa State University, ukaluara@iastate.edu

Weiwei Xie
Iowa State University, airtour101@gmail.com

Qisheng Lin
Ames Laboratory, qslin@ameslab.gov

Valentin Taufour
Iowa State University, taufour@ameslab.gov

Sergey L. Bud'ko
Iowa State University, budko@ameslab.gov

Superconductivity versus structural phase transition in the closely related $Bi_2Rh_{3.5}S_2$ and $Bi_2Rh_3S_2$

Udhara S. Kaluarachchi,[1,2] Weiwei Xie,[1,3] Qisheng Lin,[1] Valentin Taufour,[1,2] Sergey L. Bud'ko,[1,2] Gordon J. Miller,[1,3] and Paul C. Canfield[1,2]

[1]*Ames Laboratory, U.S. DOE, Iowa State University, Ames, Iowa 50011, USA*

[2]*Department of Physics and Astronomy, Iowa State University, Ames, Iowa 50011, USA*

[3]*Department of Chemistry, Iowa State University, Ames, Iowa 50011, USA*

(Received 1 April 2015; revised manuscript received 5 May 2015; published 19 May 2015)

Single crystals of $Bi_2Rh_3S_2$ and $Bi_2Rh_{3.5}S_2$ were synthesized by solution growth, and the crystal structures and thermodynamic and transport properties of both compounds were studied. In the case of $Bi_2Rh_3S_2$, a structural first-order transition at around 165 K is identified by single-crystal diffraction experiments, with clear signatures visible in resistivity, magnetization, and specific heat data. No superconducting transition for $Bi_2Rh_3S_2$ was observed down to 0.5 K. In contrast, no structural phase transition at high temperature was observed for $Bi_2Rh_{3.5}S_2$; however, bulk superconductivity with a critical temperature, $T_c \approx 1.7$ K, was observed. The Sommerfeld coefficient γ and the Debye temperature (Θ_D) were found to be 9.41 mJ mol^{-1} K^{-2} and 209 K, respectively, for $Bi_2Rh_3S_2$, and 22 mJ mol^{-1} K^{-2} and 196 K, respectively, for $Bi_2Rh_{3.5}S_2$. Study of the specific heat in the superconducting state of $Bi_2Rh_{3.5}S_2$ suggests that $Bi_2Rh_{3.5}S_2$ is a weakly coupled, BCS superconductor.

DOI: 10.1103/PhysRevB.91.174513 PACS number(s): 74.70.Dd, 74.25.−q, 61.50.Ks

I. INTRODUCTION

Superconductivity and charge density waves (CDWs) are fascinating and closely linked collective phenomena. The CDW in low-dimensional materials was first proposed by Peierls [1,2], who showed that a one-dimensional metal was unstable against a periodic lattice distortion, which creates an energy gap at the Fermi level. Superconductivity and CDW states were linked when Fröhlich proposed a mechanism of superconductivity based on a sliding, incommensurate CDW [3]. Following the formulation of the BCS theory [4] of superconductivity, it was appreciated that the superconducting state and the CDW state are both results of electron-phonon coupling often with the CDW state competing with and ultimately replacing the superconducting state as electron-phonon coupling is increased. In some, relatively rare, compounds both transitions can be found upon cooling; more often, though, a CDW or some other type of structural phase transition removes density of states at the Fermi surface and thus suppresses or even precludes the formation of a superconducting state.

It is interesting to study the properties of the materials which manifest the coexistence of superconducting and CDW states, so as to gain a better understanding of how they compete with each other for the density of states as each opens a gap at the Fermi level [5–15]. The electrical transport properties of some ternary, metal-rich chalcogenides [16–18], $A_2M_3X_2$ (A = Sn, Pb, In, Tl, and Bi; M = Co, Ni, Rh, and Pd; X = S and Se) have been reported by Natarajan and coworkers [19] with some members of this family showing superconductivity at low temperature [20–22]. Recently, Sakamoto and coworkers reported that parkerite-type $Bi_2Rh_3Se_2$ [23] was a new superconducting compound (with a critical temperature, T_c, $\sim$ 0.7 K) with a possible higher temperature CDW transition at $T_{CDW} \approx$ 250 K. Pressure studies on this compound [24] found that the resistivity anomaly at 250 K shifted to higher temperature with increasing pressure, which is unusual for a conventional CDW transition [25–27]. Given that isostructural $Bi_2Rh_3S_2$ is reported to have a resistive anomaly near 160 K (having been measured down to 77 K) [19], measurements of single crystalline $Bi_2Rh_3S_2$ to lower temperatures are called for.

Using solution growth out of a Rh-rich Rh-Bi-S melt [22], our initial growth attempts produced large grain, crystalline material that showed a clear resistivity feature near 160 K but also an apparent superconducting transition near 2 K. These results indicated that there may be some form of competition or interaction between structural phase transition and superconductivity in this ternary system. A powder x-ray diffraction measurement revealed the anticipated $Bi_2Rh_3S_2$ phase, but also indicated the presence of a second phase.

In order to better understand the physics and chemistry of this part of the Bi-Rh-S system, in this paper we present details of the crystal growth of both $Bi_2Rh_3S_2$ and a new phase: $Bi_2Rh_{3.5}S_2$, provide structural data, and present and analyze thermodynamic and transport data from each compound. Whereas $Bi_2Rh_3S_2$ manifests a first-order, structural-phase transition near 160 K and does not superconduct for $T > 0.5$ K, $Bi_2Rh_{3.5}S_2$ manifests no signs of any phase transition for 2 K $< T <$ 300 K has a significantly larger electronic specific heat coefficient, γ, and manifests bulk superconductivity below 2 K. Instead of finding the coexistence of a structural phase transition and subsequent superconductivity in one compound we found two closely related compounds: one that manifests a structural phase transition near 160 K and has a relatively lower electronic specific heat at low temperatures and another that does not undergo a structural phase transition upon cooling, has a relatively larger electronic specific heat, and does become superconducting below 2 K.

II. EXPERIMENTAL METHODS

Single crystals of $Bi_2Rh_{3.5}S_2$ and $Bi_2Rh_3S_2$ were produced using solution growth techniques [22,28,29]. For $Bi_2Rh_3S_2$, a mixture of elemental Rh, Bi, and S was placed in a 2-ml fritted

TABLE I. Lattice parameters of $Bi_2Rh_3S_2$ (293 K and 120 K) and $Bi_2Rh_{3.5}S_2$ at 293 K. All values are from single-crystal diffraction data.

Formula	$Bi_2Rh_3S_2$ (293 K)	$Bi_2Rh_3S_2$ (120 K)	$Bi_2Rh_{3.5}S_2$ (293 K)
Formula weight	790.81	790.81	842.27
Z-formula units	4	12	4
Space group	C2/m	C2/m	C2/m
a (Å)	11.291(3)	11.542(2)	11.5212(3)
b (Å)	8.378(2)	8.341(2)	7.9408(2)
c (Å)	7.942(4)	17.768(4)	7.8730(3)
β	133.286(2)°	107.614(2)°	128.033(2)°
Volume (Å^3)	546.8(3)	1630.4(5)	567.33(3)
Density (g/cm^3)	9.605	9.664	9.861

alumina crucible [30], with a molar ratio of Rh:Bi:S = 42.6:28.2:29.2, and sealed in a silica ampule under partial pressure of high-purity argon gas. The sealed ampule was heated to 1150 °C over 12 h and held there for 3 h. After that, it was cooled to 900 °C over 70 h and excess liquid was decanted using a centrifuge. For $Bi_2Rh_{3.5}S_2$, a molar ratio of Rh:Bi:S = 55:22.5:22.5 was used, heated, and cooled in a similar manner but slowly cooled to 775 °C before decanting.

Powder x-ray diffraction data were collected by using a Rigaku Miniflex II diffractometer at room temperature (Cu K_α radiation). Samples were prepared by grinding single crystals into powder and spreading them onto a thin-grease-layer-coated single-crystal Si, low-background puck. Powder x-ray diffraction data were analyzed using the GSAS [31,32] program.

Single-crystal diffraction data were measured using a Bruker Smart Apex CCD diffractometer [33] with Mo K_α radiation ($\lambda = 0.71073$ Å). Data were collected with mixed ω/ϕ scan modes and with an exposure time of 10 s per frame. The 2θ range covered from 6° to 64°. Intensities were extracted and corrected for Lorentz and polarization effects with the SAINT program. Empirical absorption corrections [34] were accomplished with SADABS, which is based on modeling a transmission surface by spherical harmonics employing equivalent reflections with $I > 3\,\sigma(I)$. Using the

TABLE II. Atomic coordinates and equivalent isotropic displacement parameters of $Bi_2Rh_3S_2$ (293 and 120 K) and $Bi_2Rh_{3.5}S_2$. All the sites are fully occupied. (U_{eq} is defined as one-third of the trace of the orthogonalized U_{ij} tensor.)

Atom	Wyck	Symm.	x	y	z	U_{eq} Å^2
$Bi_2Rh_3S_2$ (293 K)						
Bi1	4*i*	m	0.0002(1)	0	0.2518(2)	0.009(1)
Bi2	4*i*	m	0.5086(1)	0	0.2596(2)	0.012(1)
Rh1	4*f*	–1	0.25	0.25	0.5	0.009(1)
Rh2	4*i*	m	0.2472(1)	0	0.2472(2)	0.015(1)
Rh3	4*h*	2	0	0.2411(2)	0.5	0.013(1)
S	8*j*	1	0.2235(6)	0.2704(5)	0.187(1)	0.010(1)
$Bi_2Rh_3S_2$ (120 K)						
Bi1	4*i*	m	0.0709(1)	0	0.4167(1)	0.017(1)
Bi2	4*i*	m	0.2432(1)	0	0.2599(1)	0.018(1)
Bi3	4*i*	m	0.4026(1)	0	0.0830(1)	0.018(1)
Bi4	4*i*	m	0.5778(1)	0	0.4148(1)	0.017(1)
Bi5	4*i*	m	0.7383(1)	0	0.2464(1)	0.018(1)
Bi6	4*i*	m	0.9041(1)	0	0.0831(1)	0.018(1)
Rh1	8*j*	1	0.3196(2)	0.2470(3)	0.1674(1)	0.018(1)
Rh2	8*j*	1	0.4092(2)	0.2517(3)	0.3347(1)	0.017(1)
Rh3	4*i*	m	0.1550(3)	0	0.0983(2)	0.019(1)
Rh4	4*i*	m	0.1802(3)	0	0.5923(2)	0.019(1)
Rh5	4*i*	m	0.4860(3)	0	0.2499(2)	0.017(1)
Rh6	4*h*	2	0	0.2670(5)	0.5	0.018(1)
Rh7	4*e*	–1	0.25	0.25	0	0.018(1)
S1	8*j*	1	0.0187(6)	0.2265(10)	0.2464(4)	0.018(1)
S2	8*j*	1	0.1262(6)	0.2706(10)	0.0806(4)	0.019(1)
S3	8*j*	1	0.3000(6)	0.2299(9)	0.4232(4)	0.016(1)
$Bi_2Rh_{3.5}S_2$						(293 K)
Bi1	4*i*	m	0.1896(1)	0	0.1932(1)	0.009(1)
Bi2	4*i*	m	0.2525(1)	0	0.7483(1)	0.008(1)
Rh1	4*i*	m	0.0200(1)	0	0.3371(2)	0.008(1)
Rh2	2*d*	2/m	0	0.5	0.5	0.007(1)
Rh3	4*g*	2	0	−0.3114(1)	0	0.008(1)
Rh4	4*e*	–1	0.25	0.25	0	0.013(1)
S	8j	1	−0.0031(3)	−0.2889(3)	0.2908(4)	0.008(1)

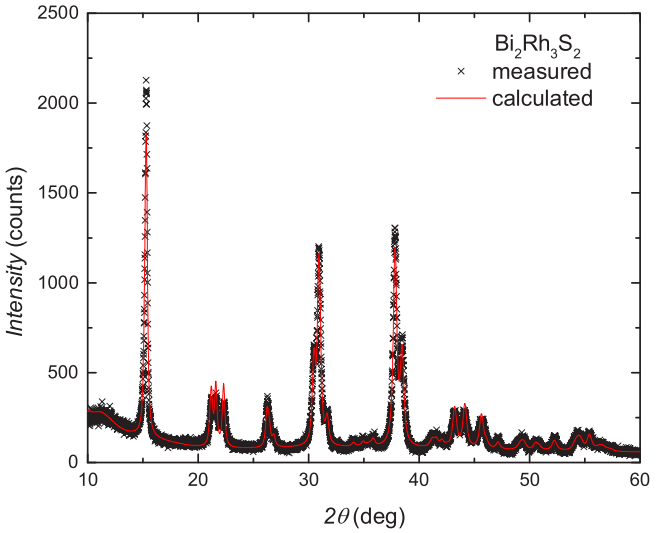

FIG. 1. (Color online) Powder diffraction pattern of pure $Bi_2Rh_3S_2$. The red line represents the calculated diffraction pattern.

SHELXTL package [35], crystal structures were solved using direct methods and refined by full-matrix least-squares on F^2. Lattice parameters were refined using single-crystal diffraction data and are summarized in Table I. Atomic coordinates and displacement parameters with fully site occupation for $Bi_2Rh_3S_2$ and $Bi_2Rh_{3.5}S_2$ are given in Table II.

The ac resistivity ($f = 17$ Hz) was measured as a function of temperature by the standard four-probe method in a Quantum Design, physical property measurement system (PPMS) instrument. Depending on the sample size Pt or Au wires (with the diameter of 25 μm or 12.7 μm, respectively) were attached to the samples using Epotek-H20E silver epoxy or DuPont 4929N silver paint. The specific heat was measured by using the relaxation method in a PPMS. The ^{3}He option was used to obtain a measurements down to 0.4 K. The DC magnetization measurements were performed in a Quantum Design, magnetic property measurement system (MPMS).

III. RESULTS

A. Phases and structures

The room temperature powder x-ray diffraction pattern from ground, phase-pure, single crystals of $Bi_2Rh_3S_2$ are shown in Fig. 1. Single crystal x-ray diffraction used to refine the lattice parameter of $Bi_2Rh_3S_2$ with monoclinic C2/m symmetry, $a = 11.291(3)$ Å, $b = 8.378(2)$ Å, $c = 7.942(4)$ Å, and $\beta = 133.286(2)^\circ$. These crystallographic parameters are within three standard deviations from literature data of $Bi_2Rh_3S_2$ [19,36]. Also these lattice parameters were used to fit the powder x-ray diffraction data shown in Fig. 1. Resistivity data measured on $Bi_2Rh_3S_2$ single crystals show only a single transition at ~165 K (see Fig. 6 below), with no superconductivity being observed down to 0.5 K.

To understand the phase transition of $Bi_2Rh_3S_2$ at 165 K, a set of single-crystal x-ray diffraction intensity data of $Bi_2Rh_3S_2$ was collected at low-temperature (LT), ca. 120 K. As shown in Fig. 2, extra diffraction spots, not belonging to the

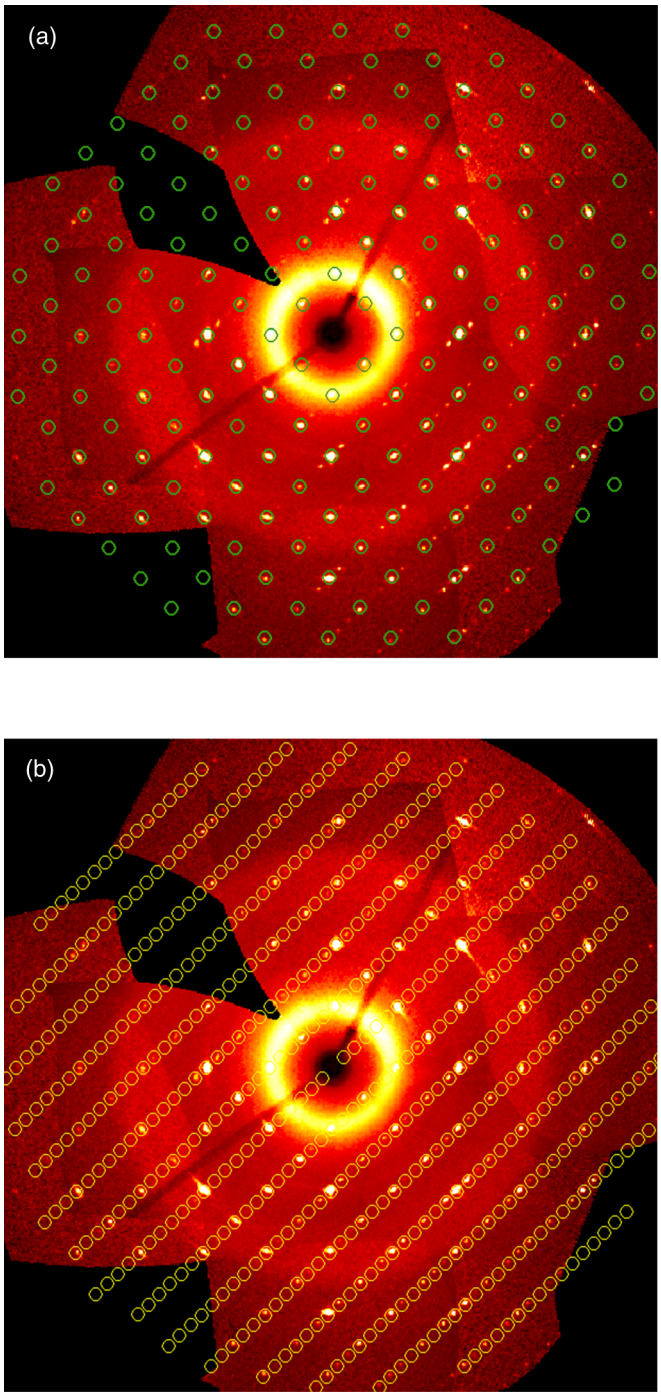

FIG. 2. (Color online) Precession images of (h 0 l) zone of a $Bi_2Rh_3S_2$ single crystal at 120 K. Green circles in (a) denote reflections that can be indexed by the base cell [C2/m, $a = 11.291(3)$ Å, $b = 8.378(2)$ Å, $c = 7.942(2)$ Å, $\beta = 133.286(2)^\circ$]; note that many reflections cannot be indexed. Yellow circles in (b) denote the reflections that can be indexed by the supercell [$a = 11.542(2)$ Å, $b = 8.341(2)$ Å, $c = 17.768(4)$ Å, $\beta = 107.614(2)^\circ$].

unit cell of $Bi_2Rh_3S_2$ at room-temperature [$a = 11.291(3)$ Å, $b = 8.378(2)$ Å, $c = 7.943(4)$ Å, $\beta = 133.286(2)^\circ$], were observed in the (h0l) zone prerecession image. However, all spots could be completely indexed by a larger monoclinic unit cell

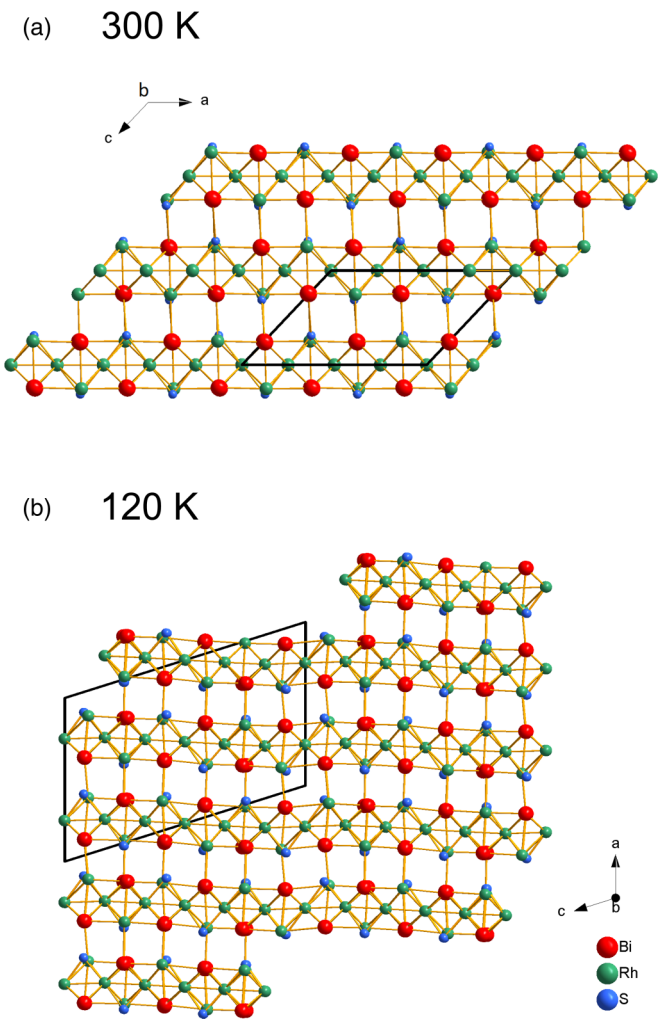

FIG. 3. (Color online) Crystal structure of $Bi_2Rh_3S_2$ at 300 K (a) and 120 K (b). The black line represents the unit cell.

[C2/m, $a = 11.542(2)$ Å, $b = 8.341(2)$ Å, $c = 17.768(4)$ Å, $\beta = 107.614(2)^\circ$], which is about three times larger than the unit cell at room temperature (RT), cf. Table I. Comparison of the RT and LT structures of $Bi_2Rh_3S_2$, shown in Fig. 3, indicate that the flat two-dimensional (2D) layers in the RT structure (parallel to ab plane) are periodically puckered in the LT superstructure.

The x-ray powder diffraction pattern of a ground, phase-pure, single crystal of $Bi_2Rh_{3.5}S_2$ is shown in Fig. 4. According to single-crystal x-ray diffraction analyses (Table I), $Bi_2Rh_{3.5}S_2$ also crystallizes in monoclinic symmetry C2/m [$a = 11.5212(3)$ Å, $b = 7.9408(2)$ Å, $c = 7.8730(3)$ Å, and $\beta = 128.033(2)^\circ$]. These lattice parameters were used to fit the powder x-ray diffraction data shown in Fig. 4. Figure 5 shows the structure of $Bi_2Rh_{3.5}S_2$ viewed along the (010) direction. Compared to the RT structure of $Bi_2Rh_3S_2$, Fig. 3(a), the 2D layers in $Bi_2Rh_{3.5}S_2$ are extensively puckered or distorted in response to the insertion of additional Rh atoms into octahedral vacancies between adjacent layers. As will be discussed below, the low-temperature electronic specific heat of $Bi_2Rh_{3.5}S_2$ is almost double that of $Bi_2Rh_3S_2$, consist with superconductivity in the former but not the latter.

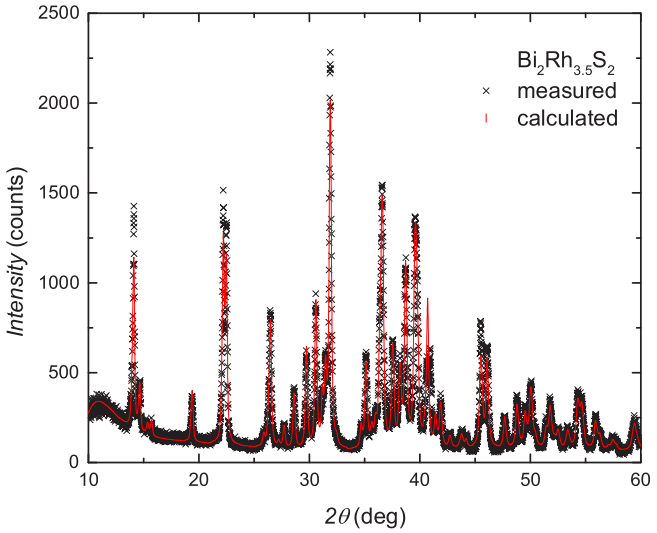

FIG. 4. (Color online) Powder diffraction pattern of $Bi_2Rh_{3.5}S_2$. The red line represents the calculated diffraction pattern.

B. Physical properties of $Bi_2Rh_3S_2$

The temperature-dependent electrical resistivity data from $Bi_2Rh_3S_2$ (Fig. 6) show a sharp feature associated with a 165 K transition with no superconducting transition observed down to 0.5 K. This material shows clear in-plane anisotropy in resistivity. Figure 6 presents the data from two samples with current flowing along each of the edge directions indicated in the lower inset. The residual resistivity ratio (RRR) values are found to be 53 and 15 in these two directions, suggesting that the in-plane scattering and/or the Fermi velocity is anisotropic. Above 170 K the resistivity increases monotonically with temperature, showing metallic behavior. Around 165 K a sudden increase or decrease of resistivity with decreasing temperature is observed in the two different, in-plane, current directions. Below 160 K, resistivity again shows metallic like behavior down to 0.5 K. The upper inset to Fig. 6 shows a 2–5 K thermal hysteresis observed in the resistivity jump near 165 K, suggesting a first-order phase transition, as confirmed by our single-crystal x-ray diffraction analyses. Whereas this behavior is typical for structural transition, it is less common for a CDW transition [7,9–14,23], which is often second

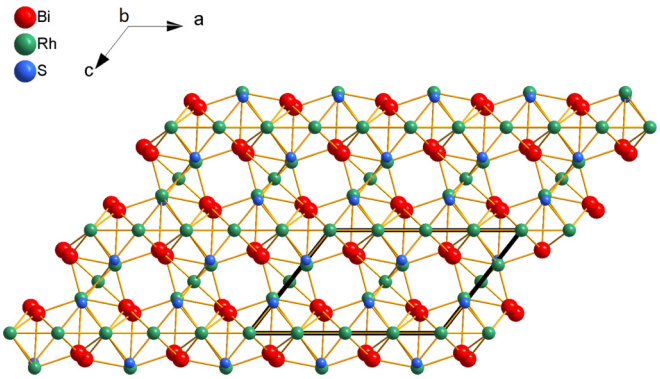

FIG. 5. (Color online) Crystal structure of $Bi_2Rh_{3.5}S_2$. The black line represents the unit cell.

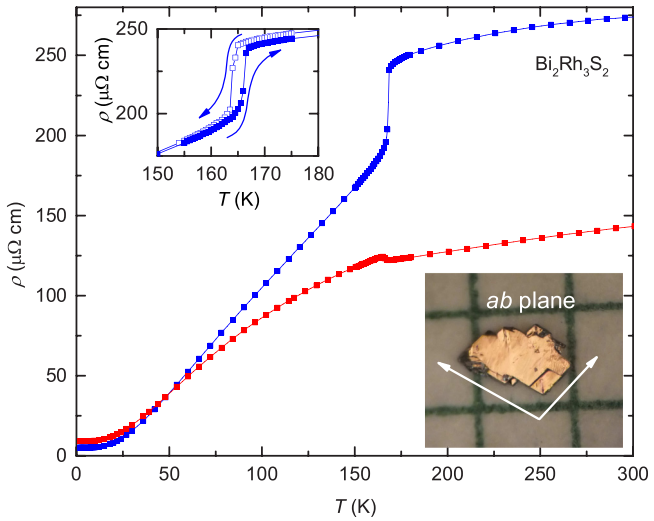

FIG. 6. (Color online) Temperature dependence of resistivity of the phase-pure $Bi_2Rh_3S_2$. The upper inset shows thermal hysteresis observed at 165 K in resistivity measurement. The lower inset shows a picture of the single crystal of $Bi_2Rh_3S_2$ on a millimeter grid. Resistivity data were measured on two different samples with current along the directions of white color arrows.

order and usually manifests an increase in resistivity due to a reduction of the density of states at the Fermi energy due to opening up of a gap in the electronic density of states at the Fermi surface. We did not observe T^2 behavior of the resistivity down to our base temperature.

Figure 7 shows the temperature dependence of the magnetic susceptibility χ(T). Since the signal from one piece of single crystal is very low and in order to measure the magnetic susceptibility, we measured the magnetization of several single crystals encapsulated in a sample holder and subtract the

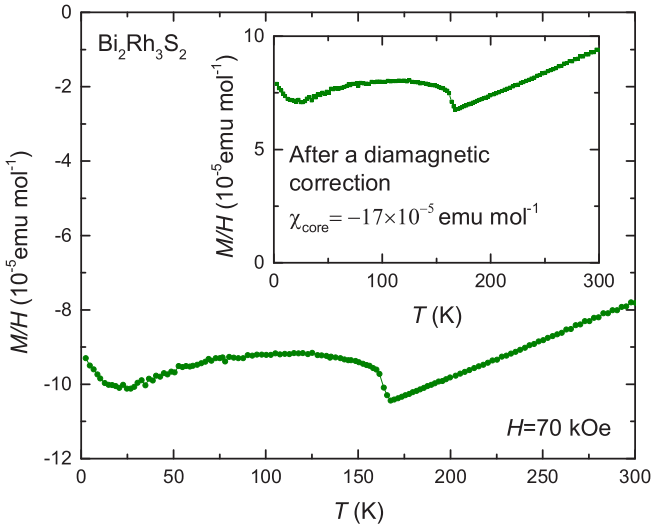

FIG. 7. (Color online) Temperature dependence of susceptibility of phase-pure $Bi_2Rh_3S_2$ before diamagnetic correction ($\chi_{core} = -17\times10^{-5}$ emu mol^{-1}) [37,38]. The inset shows after diamagnetic correction.

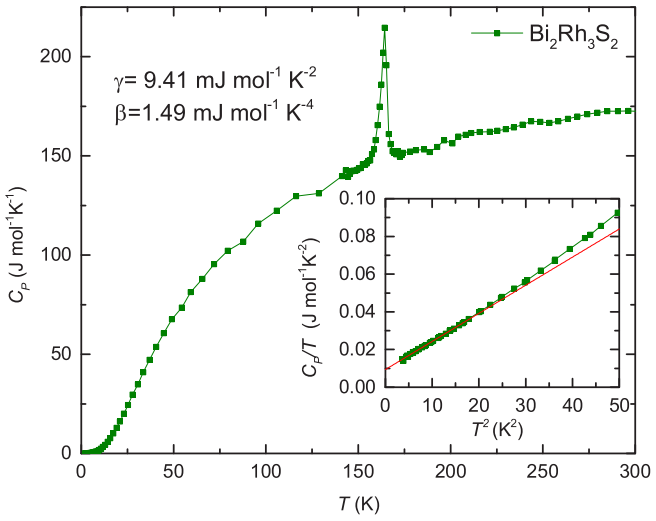

FIG. 8. (Color online) Temperature dependence of specific heat of phase-pure $Bi_2Rh_3S_2$. The lower inset represents the C_p/T vs. T^2 graph, which was used to obtain γ and β values.

background signal due to the sample holder. The negative value of the magnetic susceptibility indicates the overall diamagnetic behavior of this compound. This is due to the dominating contribution from core diamagnetism. By subtracting the core diamagnetic contribution [37,38] we can estimate the electronic contribution to the susceptibility. The inset of Fig. 7 shows the temperature dependence of the electronic contribution to the magnetic susceptibility, after the diamagnetic correction [37,38] ($\chi_{core} = -17\times10^{-5}$ emu mol^{-1}). Susceptibility linearly decreases with the decreasing temperature down to 165 K and then shows dramatic change at 165 K. Given that both Pauli paramagnetic and Landau diamagnetic susceptibility are proportional to the density of state at the Fermi level $D(\epsilon_F)$, the change in χ at 165 K is consistent with an increase in the density of state at the Fermi level $D(\epsilon_F)$. In a typical CDW material there is a reduction of the density of state at the Fermi energy due to opening up of a gap in the electronic density of states at the Fermi surface. An increase in density of state is not consistent with the CDW mechanism for structural phase transition. The low-temperature upturn (below 25 K) in the susceptibility is probably due to the presence of a small amount of paramagnetic impurities in the sample.

The temperature-dependent specific heat of $Bi_2Rh_3S_2$ (Fig. 8) shows a broadened latent heat feature, consistent with the first-order-like features seen in the resistivity and magnetization data shown in Figs. 6 and 7. The room-temperature specific heat of $Bi_2Rh_3S_2$, 172.6 J mol^{-1} K^{-1}, is close to the Dulong-Petit limit, $C_V = 3nR = 174.6$ J mol^{-1} K^{-1}. The Sommerfeld coefficient, $\gamma = 9.41$ mJ mol^{-1} K^{-2} and $\beta = 1.49$ mJ mol^{-1} K^{-4} values were obtained for the LT phase from the low-temperature data fitted with $C_p/T = \gamma + \beta T^2$, as shown in the lower inset of Fig. 8. From β we obtained a Debye temperature (Θ_D) of 209 K by using Eq. (1) and slightly larger than the value of $Bi_2Rh_3Se_2$. This reflects a higher phonon density of states at low energies, which are likely due to the presence of the lighter element "Sulfur" compared to "Selenium." A similar value of $\gamma = 9.5$ mJ mol^{-1} K^{-2} was

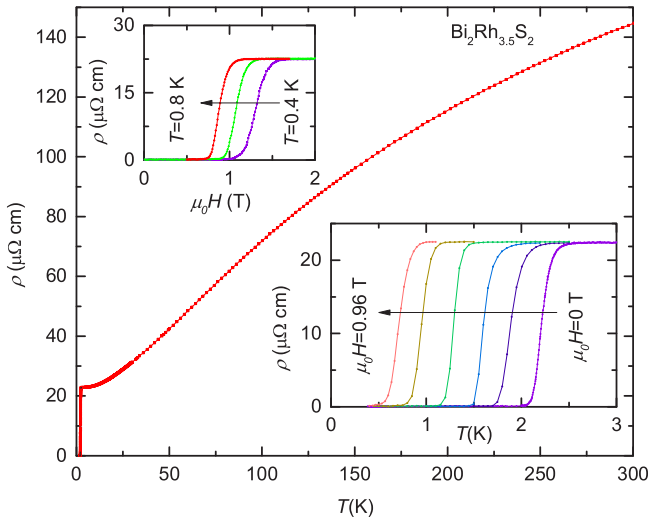

FIG. 9. (Color online) Temperature dependence of resistivity of $Bi_2Rh_{3.5}S_2$. Upper inset shows representative field scans of the resistivity at constant temperatures at 0.4 K, 0.6 K and 0.8 K. Lower inset shows representative temperature scans of the resistivity at constant fields at 0 T, 0.08 T, 0.18 T, 0.42 T, 0.74 T and 0.96 T.

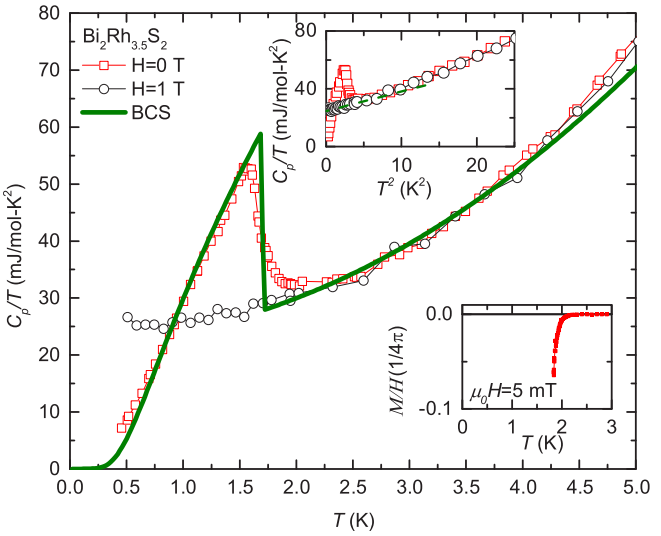

FIG. 10. (Color online) Low-temperature C_p/T vs. T of $Bi_2Rh_{3.5}S_2$. Red open squares represent zero-field measurements, while black open circles represent measurements under 1 T field. Green color solid line shows the BCS calculation. The upper inset represents the C_p/T vs. T^2 graph, which was used to obtain γ and β values. Lower inset shows ZFC M/H data of $Bi_2Rh_{3.5}S_2$.

obtained in isostructural $Bi_2Rh_3Se_2$ compound [23]:

$$\Theta_D = \left(\frac{12\pi^2 nR}{5\beta}\right)^{1/3}. \quad (1)$$

With our measurements of single-crystal diffraction, resistivity, magnetization, and the specific heat, we can conclude the phase transition in $Bi_2Rh_3S_2$ at 165 K is a first-order structural phase transition. We do not have clear evidence of a CDW being associated with this transition.

In the case of $Bi_2Rh_3Se_2$, based on the results of the resistivity, magnetization, thermoelectric power, thermal expansion, and low-temperature x-ray measurements, Sakamoto *et al.* [23] conclude that the anomaly at ∼250 K is a CDW transition. However, Chen *et al.* [24] report that, based on their experiments of pressure and selected-area electron diffraction study, phase transition at ∼250 K is not a CDW transition, rather a structural transition. In the present case of $Bi_2Rh_3S_2$, further advanced measurements would be needed to find any support for a possible CDW.

C. Physical properties of $Bi_2Rh_{3.5}S_2$

Figure 9 presents the temperature dependence of resistivity of $Bi_2Rh_{3.5}S_2$, which, unlike $Bi_2Rh_3S_2$, does not show any transitions in the resistivity data around 165 K. However, it does manifest zero resistivity below 2 K, indicating an onset of a superconducting transition at this temperature. RRR of $Bi_2Rh_{3.5}S_2$ is 6.4, less than the RRR of $Bi_2Rh_3S_2$. We did not observe T^2 behavior in resistivity down to the base temperature of our measurement.

Figure 10 shows the low temperature specific heat data of $Bi_2Rh_{3.5}S_2$. The open red squares represent zero-field measurements, whereas the open black circles represent measurements under 1 T magnetic field, i.e., $H \geqslant H_{c2}(T)$ for the measured temperature range (see below). From the low-temperature data fitted with $C_p/T = \gamma + \beta T^2$ from 2 to 3.8 K, as shown in the upper inset of Fig. 10, we find $\gamma = 22$ mJ mol^{-1} K^{-2} and $\beta = 1.94$ mJ mol^{-1} K^{-4} and can infer that $\Theta_D = 196$ K. We can clearly see that γ of the superconducting $Bi_2Rh_{3.5}S_2$ is twice as large as that for the nonsuperconducting $Bi_2Rh_3S_2$ or $Bi_2Rh_3Se_2$ [23]. Also, this value is larger than the other reported parkerite-type superconductors, $Bi_2Ni_3S_2$ [20], $Bi_2Ni_3Se_2$ [20], and $Bi_2Pd_3Se_2$ [21].

On one hand, $T_c = 1.7$ K was obtained by using an equal entropy construction to the low-temperature specific-heat data. On the other hand, the $H = 0$ $C_p(T)$ data start to separate from the $H = 1$ T $C_p(T)$ data below 2.2 K. Specific-heat jump of $\Delta C = 52.4$ mJ mol^{-1} K^{-1} gives $\Delta C/\gamma T_c = 1.39$, which is close to the BCS value 1.43 for a weak-coupling superconductor. The green-colored solid line represents a BCS [4,39] calculation. The deviation above 4 K, normal-state data from the simple Debye model indicates the presence of at least a T^5 term in the lattice contribution.

The lower inset of Fig. 10 shows zero-field-cooled (ZFC) data of $Bi_2Rh_{3.5}S_2$. We were not able to see the full transition in ZFC measurements because the minimum temperature that we can reach in the MPMS is 1.8 K. These data are consistent with the broadened transition seen in the resistivity and the $C_p(T)$ data.

The upper inset of Fig. 9 shows the field dependence of the superconducting transition for temperatures from 0.4 to 0.8 K and the lower inset shows the temperature dependence of the superconducting transition from 0 to 0.96 T applied field. Figure 11 shows $\mu_0 H_{c2}$(T) as a function of the critical temperature determined from the resistivity data. Lower and upper insets show the maximum slope of the resistivity extrapolated to $\rho = 0$, used as a criteria to obtain the $\mu_0 H_{c2}$ and T_c, respectively. We can estimate the Ginzburg-Landau (GL) coherence length [39] at zero temperature, $\xi(0) = 150$ Å

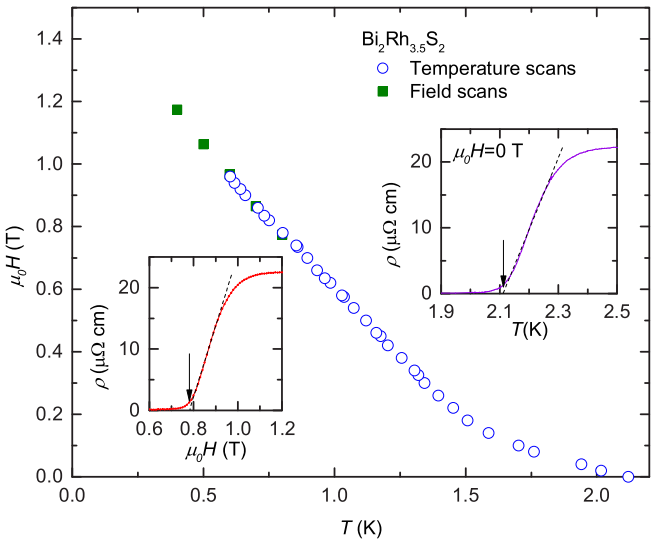

FIG. 11. (Color online) Temperature dependence of the upper critical field for $Bi_2Rh_{3.5}S_2$ determined from the resistivity data. Lower and upper insets show the criteria (maximum slope extrapolated to $\rho = 0$), which was used to obtain the data points.

by using the relation $\mu_0 H_{c2}(0) = \Phi_0/2\pi\xi(0)^2$, in which Φ_0 is the quantum flux and estimating $\mu_0 H_{c2}(0)$ to be 1.5 T. The value of $\mu_0 H_{c2}(0)$ is well below the Pauli paramagnetic limit [40] of $\mu_0 H_{c2}^p(0) = 1.85\,T_c = 3.15$ T, suggesting an orbital pair-breaking mechanism. The upward curvature near T_c in the $H_{c2}(T)$ data shown in Fig. 11 may come from a distribution of T_c values in the sample [41–44] or multiband superconductivity as was discussed by Shulga *et al.* [45] or nonlocal correction [46,47] to the Ginzburg-Landau equations. Similar H_{c2}(T) curvatures were found for YNi_2B_2C as well as $LuNi_2B_2C$ [45].

The electron-phonon coupling constant $\lambda_{\text{e-ph}}$ can be estimated from the McMillan equation [48] for the superconducting transition temperature [Eq. (2)], for phonon-mediated superconductors,

$$T_c = \frac{\Theta_D}{1.45}\exp\left[-\frac{1.04(1+\lambda_{\text{e-ph}})}{\lambda_{\text{e-ph}} - \mu^*(1+0.62\lambda_{\text{e-ph}})}\right], \quad (2)$$

where μ^*, the Coulomb pseudopotential, having value often between 0.1 and 0.2 and usually taken as 0.13 [48]. Similar values of μ^* have been used in isostructural compounds [20,21,23]. Using $\Theta_D = 196$ K and $T_c = 1.7$ K we estimated $\lambda_{\text{e-ph}} = 0.54$. A difference of μ from the assumed value of 0.13 will give a different value of $\lambda_{\text{e-ph}}$. For example, $\lambda_{\text{e-ph}} = 0.48$ if $\mu = 0.1$ and $\lambda_{\text{e-ph}} = 0.69$ if $\mu = 0.2$. By using both normal state and superconducting state specific heat data, one can obtain the thermodynamic critical field, $\mu_0 H_c(0)$ as a function of temperature from Eq. (3),

$$\frac{\mu_0 V_m H_c(0)^2}{2} = \int_0^{T_c} \Delta S(T')dT', \quad (3)$$

in which $\Delta S(T)$ is the entropy difference between the normal and superconducting states and V_m (8.54×10^{-5} m^3 mol^{-1}) is the molar volume. The calculated value of $\mu_0 H_c(0)$ is 23 mT for $Bi_2Rh_{3.5}S_2$. This value is larger than the value of $Bi_2Rh_3Se_2$ and clearly reflects the larger γ and T_c of $Bi_2Rh_{3.5}S_2$:

$$\mu_0 H_c(0) = 1.76\times10^{-4}\,[4\pi D(\epsilon_F)]^{1/2}\,k_B T_c, \quad (4a)$$

$$\frac{\gamma}{V_m} = \frac{1}{15}\pi^2 D(\epsilon_F) k_B^2, \quad (4b)$$

$$\mu_0 H_c(0) = 1.76\left(\frac{6\gamma\mu_0}{4\pi^2 V_m}\right)^{1/2} T_c. \quad (4c)$$

Using BCS theory results [4] [Eqs. (4a) and (4b)] we can eliminate the $D(\epsilon_F)$ term and, for the limit of an isotropic gap function, use Eq. (4c) to calculate the value of $\mu_0 H_c(0) = 21$ mT. This value is close to the calculated value using specific heat.

Also the penetration depth $\lambda(0)$ and GL parameter κ are found to be 7450 Å and 50 from Eqs. (5) and (6), respectively:

$$\mu_0 H_c(0) \approx \frac{\Phi_0}{2\sqrt{2}\lambda(0)\xi(0)}, \quad (5)$$

$$\kappa \approx \frac{\lambda(0)}{\xi(0)}. \quad (6)$$

From the specific heat jump and using Rutger's relation, $\Delta C/T_c = (1/8\pi\kappa^2)(dH_{c2}/dT)^2|_{T_c}$ [49], one can obtain a similar κ value of 30. The obtained $\lambda(0)$ and κ values of $Bi_2Rh_{3.5}S_2$ are smaller than the values of $Bi_2Rh_3Se_2$ [23], but the value of κ ($\kappa > 1/\sqrt{2}$) is large enough to consider $Bi_2Rh_{3.5}S_2$ is a type II superconductor.

IV. CONCLUSIONS

Single crystals of the closely related $Bi_2Rh_3S_2$ and $Bi_2Rh_{3.5}S_2$ systems were synthesized by high-temperature solution growth. Resistivity, magnetization, and specific heat measurements were carried out to characterize their normal states and, for $Bi_2Rh_{3.5}S_2$, superconducting properties. $Bi_2Rh_3S_2$ manifests a structural phase transition around 165 K. No superconductivity was observed down to 0.5 K. Single-crystal diffraction measurements at 120 and 300 K confirmed that a threefold superstructure develops. We noticed a large, in-plane, resistivity anisotropy in this compound. Thermal hysteresis and the specific heat feature at 165 K are consistent with a first-order phase transition. The Sommerfeld coefficient $\gamma = 9.41$ mJ mol^{-1} K^{-2} and the Debye temperature = 209 K were calculated by using low-temperature specific-heat data. Based on our measurements, we do not have evidence of a CDW-type mechanism being responsible for this transition.

$Bi_2Rh_{3.5}S_2$ adopts a monoclinic (C/2m) crystal structure. This material shows a signature of superconductivity in the resistivity and specific-heat measurements consistent with bulk superconductivity below the critical temperature T_c of 1.7 K. The calculated values for the Sommerfeld coefficient and the Debye temperature are 22 mJ mol^{-1} K^{-2} and 196 K respectively. Analysis of the jump in the specific heat at T_c, suggest that $Bi_2Rh_{3.5}S_2$ as a weak electron-phonon coupled, BCS superconductor.

ACKNOWLEDGMENTS

We thank W. Straszheim, A. Jesche, X. Lin, H. Kim, E. Mun, and M. Tanatar for experimental assistance and

T. Kong, S. Ran, H. Hodovanets, and V. G. Kogan for useful discussions. Part of this work (U.S.K., V.T.) was carried out at Iowa State University and supported by AFOSR-MURI Grant No. FA9550-09-1-0603. Part of this work (W.X., Q.L., G.J.M., S.L.B., P.C.C.) was performed at the Ames Laboratory, U.S. DOE, under Contract No. DE-AC02-07CH11358.

[1] R. Peierls, Ann. Phys. **396**, 121 (1930).
[2] R. E. Peierls, *Quantum Theory of Solids* (Clarendon, Oxford, 1955).
[3] H. Fröhlich, P. Roy. Soc. A-Math. Phys. **223**, 296 (1954).
[4] J. Bardeen, L. N. Cooper, and J. R. Schrieffer, Phys. Rev. **108**, 1175 (1957).
[5] A. M. Gabovich and A. I. Voitenko, Low. Temp. Phys. **26**, 305 (2000).
[6] A. M. Gabovich, A. I. Voitenko, J. F. Annett, and M. Ausloos, Supercond. Sci. Tech. **14**, R1 (2001).
[7] J. A. Wilson, F. J. Di Salvo, and S. Mahajan, Phys. Rev. Lett. **32**, 882 (1974).
[8] J. Harper, T. Geballe, and F. D. Salvo, Phys. Lett. A **54**, 27 (1975).
[9] P. Monceau, N. P. Ong, A. M. Portis, A. Meerschaut, and J. Rouxel, Phys. Rev. Lett. **37**, 602 (1976).
[10] F. J. Di Salvo, D. E. Moncton, and J. V. Waszczak, Phys. Rev. B **14**, 4321 (1976).
[11] R. N. Shelton, L. S. Hausermann-Berg, P. Klavins, H. D. Yang, M. S. Anderson, and C. A. Swenson, Phys. Rev. B **34**, 4590 (1986).
[12] B. Becker, N. G. Patil, S. Ramakrishnan, A. A. Menovsky, G. J. Nieuwenhuys, J. A. Mydosh, M. Kohgi, and K. Iwasa, Phys. Rev. B **59**, 7266 (1999).
[13] S. Ramakrishnan, Pramana **58**, 827 (2002).
[14] Y. Singh, D. Pal, S. Ramakrishnan, A. M. Awasthi, and S. K. Malik, Phys. Rev. B **71**, 045109 (2005).
[15] E. Morosan, H. W. Zandbergen, B. S. Dennis, J. W. G. Bos, Y. Onose, T. Klimczuk, A. P. Ramirez, N. P. Ong, and R. J. Cava, Nat. Phys. **2**, 544 (2006).
[16] C. Michener and M. Peacock, Am. Mineral **28**, 343 (1943).
[17] M. Peacock and J. McAndrew, Am. Mineral **35**, 425 (1950).
[18] W. Brower, H. Parker, and R. Roth, Am. Mineral **59**, 296 (1974).
[19] S. Natarajan, G. Rao, R. Baskaran, and T. Radhakrishnan, J. Less-Common. Met. **138**, 215 (1988).
[20] T. Sakamoto, M. Wakeshima, and Y. Hinatsu, J. Phys.: Condens. Matter **18**, 4417 (2006).
[21] T. Sakamoto, M. Wakeshima, Y. Hinatsu, and K. Matsuhira, Phys. Rev. B **78**, 024509 (2008).
[22] X. Lin, S. L. Bud'ko, and P. C. Canfield, Philos. Mag. **92**, 2436 (2012).
[23] T. Sakamoto, M. Wakeshima, Y. Hinatsu, and K. Matsuhira, Phys. Rev. B **75**, 060503 (2007).
[24] C. Chen, C. Chan, S. Mukherjee, C. Chou, C. Tseng, S. Hsu, M.-W. Chu, J.-Y. Lin, and H. Yang, Solid. State. Commun. **177**, 42 (2014).
[25] C. W. Chu, V. Diatschenko, C. Y. Huang, and F. J. DiSalvo, Phys. Rev. B **15**, 1340 (1977).
[26] A. Briggs, P. Monceau, M. Nunez-Regueiro, J. Peyrard, M. Ribault, and J. Richard, J. Phys. C: Solid State **13**, 2117 (1980).
[27] S. L. Bud'ko, T. A. Wiener, R. A. Ribeiro, P. C. Canfield, Y. Lee, T. Vogt, and A. H. Lacerda, Phys. Rev. B **73**, 184111 (2006).
[28] P. C. Canfield and Z. Fisk, Philos. Mag. B **65**, 1117 (1992).
[29] P. C. Canfield and I. R. Fisher, J. Crystal Growth **225**, 155 (2001).
[30] C. Petrovic, P. C. Canfield, and J. Y. Mellen, Philos. Mag. **92**, 2448 (2012).
[31] B. H. Toby, J. Appl. Crystal. **34**, 210 (2001).
[32] A. C. Larson and R. B. Von Dreele, *General Structure Analysis (GSAS)*, Los Alamos National Laboratory Report LAUR 86-748 (2000).
[33] *SMART version 5*, Bruker AXS, Madison WI, smart version 5 ed. (2003).
[34] R. H. Blessing, Acta. Crystallogr. A **51**, 33 (1995).
[35] G. Sheldrick, Bruker AXS, Madison, WI, shelx, version 5.1 ed. (2002).
[36] I. Anusca, A. Schmid, P. Peter, J. Rothballer, F. Pielnhofer, and R. Weihrich, Z. Anorg. Allg. Chem. **635**, 2410 (2009).
[37] E. A. Boudreaux and L. N. Mulay, *Theory and Applications of Molecular Paramagnetism* (John Wiley and Sons, New York, 1976).
[38] G. A. Bain and J. F. Berry, J. Chem. Educ. **85**, 532 (2008).
[39] M. Tinkham, *Introduction to Superconductivity*, 2nd ed. (Dover Publications, New York, 1996).
[40] A. M. Clogston, Phys. Rev. Lett. **9**, 266 (1962).
[41] T. Park, E. Park, H. Lee, T. Klimczuk, E. D. Bauer, F. Ronning, and J. D. Thompson, J. Phys.: Condens. Matter **20**, 322204 (2008).
[42] H. Xiao, T. Hu, A. P. Dioguardi, N. apRoberts-Warren, A. C. Shockley, J. Crocker, D. M. Nisson, Z. Viskadourakis, X. Tee, I. Radulov, C. C. Almasan, N. J. Curro, and C. Panagopoulos, Phys. Rev. B **85**, 024530 (2012).
[43] H. Xiao, T. Hu, S. K. He, B. Shen, W. J. Zhang, B. Xu, K. F. He, J. Han, Y. P. Singh, H. H. Wen, X. G. Qiu, C. Panagopoulos, and C. C. Almasan, Phys. Rev. B **86**, 064521 (2012).
[44] A. Ślebarski, M. Fijałkowski, M. M. Maśka, M. Mierzejewski, B. D. White, and M. B. Maple, Phys. Rev. B **89**, 125111 (2014).
[45] S. V. Shulga, S.-L. Drechsler, G. Fuchs, K.-H. Müller, K. Winzer, M. Heinecke, and K. Krug, Phys. Rev. Lett. **80**, 1730 (1998).
[46] P. C. Hohenberg and N. R. Werthamer, Phys. Rev. **153**, 493 (1967).
[47] V. Metlushko, U. Welp, A. Koshelev, I. Aranson, G. W. Crabtree, and P. C. Canfield, Phys. Rev. Lett. **79**, 1738 (1997).
[48] W. L. McMillan, Phys. Rev. **167**, 331 (1968).
[49] U. Welp, W. K. Kwok, G. W. Crabtree, K. G. Vandervoort, and J. Z. Liu, Phys. Rev. Lett. **62**, 1908 (1989).